Data Driven Fault Detection and Identification of Wind Turbines

Jianfei Dong
j.dong@tudelft.nl

Michel Verhaegen
m.verhaegen@moesp.org

Jan-Willem van Wingerden
j.w.vanwingerden@tudelft.nl

Delft Center for Systems and Control, Delft University of Technology, Delft, The Netherlands

Abstract

This paper applies a novel data driven fault detection and identification (FDI) approach to large-scale wind turbines. This new approach directly links subspace identification with fault detection and identification filter designs. Physical modeling of a wind turbine is bypassed. The FDI filters are directly identified from the input and output (I/O) signals measured on the fault-free wind turbine; and therefore provide more usability to their practitioners. The nonlinear dynamics of the wind turbine are converted into a linear time invariant (LTI) model via inverse Coleman transformation. The data driven FDI approach for LTI systems can hence be applied without linearizing the nonlinear model. The simulation results verify the effectiveness of the data driven FDI designs for detecting and estimating additive sensor faults on the wind turbine.

Keywords: fault detection and identification, subspace identification, data-driven methods.

1 Introduction

Generating electricity from wind has become a reality in recent years. In fact, the authors of this paper are frequently encouraged by their electricity providers to subscribe to the supply from wind turbines. In the Netherlands, the modern wind turbines are joining the traditional wind mills as new landmarks.

However, potential faults of wind turbines can occur in their gearbox, blades, sensors, and the motors yawing the rotor. These faults cause remarkable downtime of a wind turbine. The maintenance of a wind turbine, where these faults has occurred, is actually a big challenge for industrial practitioners, especially for offshore large-scale wind turbines. The challenge can actually be attributed to the difficulty and even the danger in accessing the turbines. This hence necessitates the availability of automatic detection (also known as condition monitoring in the literature) and identification of the faults and reconfiguration of the control system accordingly.

In the existing literature, condition monitoring of wind turbines has been developed based on signal processing and artificial intelligence (AI) techniques, e.g. [1, 2]. Signal processing is to extract features from measured data; while AI is used to classify the features to different conditions. This is also known as a “black-box” approach. However, black-box approaches usually suffer from lacking the robustness against unseen data. On the other hand, for a dynamic process, the initial state and control signals largely influence the readings from sensors. Black-box methods cope with this variations by performing as many experiments as possible. An alternative way is of course to rely on the dynamic model of a wind turbine, which take the initial state and control signals into account. This is the so-called “model-based” approaches, e.g. [3].

Generally, modeling by first principles is a time-consuming and expensive task. This is especially true for such a large-scale system as a wind turbine. An alternative way is to use system identification techniques [4], which models based on data. In fact, the model used for FDI design in [3] was identified from data. However, with system identification, a model still has to be built before the FDI design tasks can actually be carried out. A more user friendly approach should avoid the modeling step, and directly design the FDI filters from data. Obviously, the less the intermediate steps, the more the usability of the approach. Inspired by this, [5, 6] have recently developed a new approach for directly synthesizing FDI filters from data; i.e. the Fault detection and Identification approach Connected to Subspace Identification, or FICSI. It is the purpose of this paper to apply this approach on wind turbines.

The rest of the paper is organized as follows. We first introduce the wind turbine model considered throughout the paper. The data driven FDI algorithm is then developed for this system. Simulation experiments are finally presented, where the parameterized nonlinear wind turbine model as introduced in Section 2 play the role of a real turbine. The results verify the effectiveness of the proposed methodology in detecting and estimating additive sensor faults on the wind turbine.

2 Wind turbine model

2.1 Physical wind turbine model

In this paper, we consider a seven degrees of freedom (DOF) model as described in [7] and [8]. The model de-

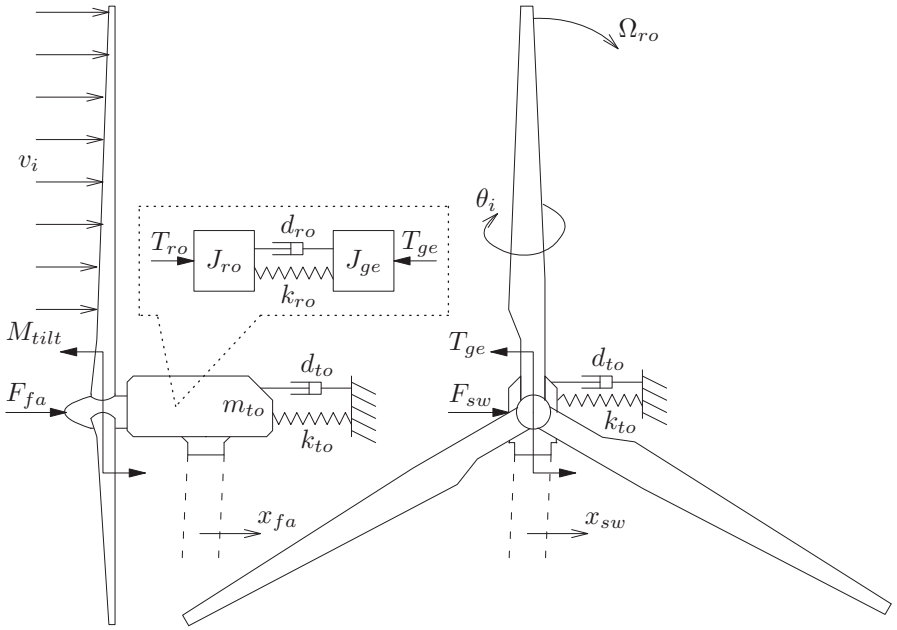

Figure 1: Schematic representation of the wind turbine model.

scribes the rotational dynamics of a wind turbine around a particular operating point. The model contains the DOFs for the main rotation, first torsion mode of the drive train, the first fore-aft, and sideward bending mode of the tower. In this model the blades are considered to be rigid. In Figure 1, a schematic representation of the model is illustrated.

Using a linearized conversion of the aerodynamic behavior, the model equations can be written in the following continuous time nonlinear form:

$$\begin{aligned} \dot{x} &= Ax + \left(B^{(1)} + \sum_{i=1}^{3} B^{(i+1)} \varphi^{(i)} \right) u \qquad (1) \\ &+ \left(F^{(1)} + \sum_{i=1}^{3} F^{(i+1)} \varphi^{(i)} \right) v, \\ y &= \left(C^{(1)} + \sum_{i=1}^{3} C^{(i+1)} \varphi^{(i)} \right) x + Du + Gv, \quad (2) \end{aligned}$$

where the matrices $B^{(i)}$, $C^{(i)}$, and $F^{(i)}$ are multiplied with the azimuth angle $\varphi^{(i)}$ of the accompanying rotor blade. The wind turbine model under consideration has three rotor blades $(i = 1, 2, 3)$ and is normally used to design individual pitch controllers. The system state, input, disturbance, and output vector are given by:

$$\begin{aligned} x &= \left[\begin{array}{ccccccc} \delta\Omega_{ro}, & x_{fa}, & \dot{x}_{fa}, & x_{sw}, & \dot{x}_{sw}, & \varepsilon, & \dot{\varepsilon} \end{array} \right]^T, \\ u &= \left[\begin{array}{cccc} \delta\theta_1, & \delta\theta_2, & \delta\theta_3, & \delta T_{ge} \end{array} \right]^T, \\ v &= \left[\begin{array}{ccc} \delta v_1, & \delta v_2, & \delta v_3 \end{array} \right]^T, \\ y &= \left[\begin{array}{cccccc} \delta\Omega_{ge}, & \dot{x}_{fa}, & \dot{x}_{sw}, & \delta M_1, & \delta M_2, & \delta M_3 \end{array} \right]^T, \end{aligned}$$

respectively. This model contains thus the control inputs for the variation in generator torque δT_{ge} and the pitch angle $\delta\theta_i$ of each rotor blade. Furthermore, the model contains the inputs for the wind speed disturbance δv_i on each of the three rotor blades. The outputs are the variations in generator speed $\delta\Omega_{ge}$, the fore-aft velocity $\dot{x}_{fa}$ and sideward velocity $\dot{x}_{sw}$ of the tower, and the blade root bending moment δM_i of each rotor blade. The state contains the variations in rotor speed $\delta\Omega_{ro}$, the fore-aft displacement x_{fa} and velocity $\dot{x}_{fa}$, the sideward displacement x_{sw} and velocity $\dot{x}_{sw}$, and the drive-train displacement ε and speed $\dot{\varepsilon}$.

The model under consideration has a constant A matrix while the input and output matrices depend on the azimuth angle, φ. In [7] the Coleman transformation is used to transform this model to an LTI model. The Coleman transformation is a nonlinear transformation that is used to transform the outputs defined in the rotating frame to the fixed non-rotating frame. In a similar way this can be done for the inputs. For brevity, we shall only give the transformed LTI model in the Coleman domain, while refer to the detailed representations of $\{A, B^{(j)}, F^{(j)}, C^{(j)}, D, W | j = 1, \cdots, 4\}$ in [7, 8]; i.e.

$$\begin{aligned} \dot{x}_{cm} &= A_{cm} x_{cm} + B_{cm} u_{cm} + F_{cm} v_{cm}, \qquad (3) \\ y_{cm} &= C_{cm} x_{cm} + D_{cm} u_{cm} + W_{cm} v_{cm}, \qquad (4) \end{aligned}$$

where the matrices are defined in (5). The I/Os and disturbances in the Coleman domain are defined as follows, where the signals $\delta T_{ge}, \delta\Omega_{ge}, \dot{x}_{fa}, \dot{x}_{sw}$ are not transformed.

$$\begin{aligned} u_{cm} &= \left[\begin{array}{cccc} \delta\theta_{cm1} & \delta\theta_{cm2} & \delta\theta_{cm3} & \delta T_{ge} \end{array} \right]^T, \\ v_{cm} &= \left[\begin{array}{ccc} \delta v_{cm1} & \delta v_{cm2} & \delta v_{cm3} \end{array} \right]^T, \\ y_{cm} &= \left[\begin{array}{cccccc} \delta\Omega_{ge} & \dot{x}_{fa} & \dot{x}_{sw} & \delta M_{cm1} & \delta M_{cm2} & \delta M_{cm3} \end{array} \right]^T. \end{aligned}$$

In the parametric matrices the parameters k_{Mx}, k_{Mz}, k_{Fx}, and k_{Fz} describe the aerodynamic gains from the pitch angle to the root moment, flap moment, root force, and flap force, respectively. The parameters h_{Mx}, h_{Mz}, h_{Fx}, and h_{Fz} describe the gain from the wind speed to the root moment, flap moment, root force, and flap force,

$$
\begin{aligned}
A_{cm} &= \begin{bmatrix}
0 & 0 & -\frac{3hMx}{J_{ro}} & 0 & 0 & -\frac{k_{ro}}{J_{ro}} & -\frac{d_{ro}}{J_{ro}} \\
0 & 0 & 1 & 0 & 0 & 0 & 0 \\
0 & -\frac{k_{to}}{m_{to}} & -\frac{d_{to}}{m_{to}} - \frac{3h_{Fx}}{m_{to}} + \frac{81Rh_{Mz}}{32H^2m_{to}} & 0 & 0 & 0 & 0 \\
0 & 0 & 0 & 0 & 1 & 0 & 0 \\
0 & 0 & \frac{27Rh_{Fz}}{16Hm_{to}} & -\frac{k_{to}}{m_{to}} & -\frac{d_{to}}{m_{to}} & 0 & 0 \\
0 & 0 & 0 & 0 & 0 & 0 & 1 \\
0 & 0 & -\frac{3h_{Mx}}{J_{ro}} & 0 & 0 & -\frac{J_{ro}+J_{ge}}{J_{ro}J_{ge}}k_{ro} & -\frac{J_{ro}+J_{ge}}{J_{ro}J_{ge}}d_{ro}
\end{bmatrix}, \\
B_{cm} &= \begin{bmatrix}
\frac{3k_{Mx}}{J_{ro}} & 0 & 0 & 0 \\
0 & 0 & 0 & 0 \\
-\frac{3k_{Fx}}{m_{to}} & -\frac{9k_{Mz}}{4Hm_{to}} & 0 & 0 \\
0 & 0 & 0 & 0 \\
0 & -\frac{3k_{Fz}}{2m_{to}} & 0 & \frac{3}{2Hm_{to}} \\
0 & 0 & 0 & 0 \\
\frac{3k_{Mx}}{J_{ro}} & 0 & 0 & \frac{1}{J_{ge}}
\end{bmatrix}, F_{cm} = \begin{bmatrix}
\frac{3h_{Mx}}{J_{ro}} & 0 & 0 \\
0 & 0 & 0 \\
\frac{3h_{Fx}}{m_{to}} & \frac{9h_{Mx}}{4Hm_{to}} & 0 \\
0 & 0 & 0 \\
0 & -\frac{3h_{Fz}}{2m_{to}} & 0 \\
0 & 0 & 0 \\
\frac{3h_{Mx}}{J_{ro}} & 0 & 0
\end{bmatrix}, W_{cm} = \begin{bmatrix}
0 & 0 & 0 \\
0 & 0 & 0 \\
0 & 0 & 0 \\
h_{Mz} & 0 & 0 \\
0 & h_{Mz} & 0 \\
0 & 0 & h_{Mz}
\end{bmatrix}, \\
C_{cm} &= \begin{bmatrix}
1 & 0 & 0 & 0 & 0 & 0 & -1 \\
0 & 0 & 1 & 0 & 0 & 0 & 0 \\
0 & 0 & 0 & 0 & 1 & 0 & 0 \\
0 & 0 & -h_{Mz} & 0 & 0 & 0 & 0 \\
0 & 0 & \frac{9Rh_{Mz}}{8H} & 0 & 0 & 0 & 0 \\
0 & 0 & 0 & 0 & 0 & 0 & 0
\end{bmatrix}, D_{cm} = \begin{bmatrix}
0 & 0 & 0 & 0 \\
0 & 0 & 0 & 0 \\
0 & 0 & 0 & 0 \\
k_{Mz} & 0 & 0 & 0 \\
0 & k_{Mz} & 0 & 0 \\
0 & 0 & k_{Mz} & 0
\end{bmatrix}.
\end{aligned} \tag{5}
$$

respectively. The constants R and H are the rotor radius and the height of the hub, respectively; the mass moment of inertia J, the mass m, the stiffness k and the damping d. Furthermore, the subscripts ro, to, and ge refer to the rotor, tower, and generator, respectively. The aerodynamic constants are listed in Table 1 and are derived for a wind speed of $16\ \mathrm{m/s}$, a pitch angle of 10 degrees, and a rotor speed of $1.795\ \mathrm{rad/s}$.

Table 1: Numerical values of the model parameters [8].

parameter	value
H	55.953 m
R	40 m
J_{ge}	1.067×10^6 kgm^2
J_{ro}	7.187×10^6 kgm^2
k_{ro}	1.262×10^8 N/m
d_{ro}	1.262×10^5 Ns/m
m_{to}	1.5657×10^5 kg
k_{to}	1.235×10^6 N/m
d_{to}	2.7995×10^3 Ns/m
h_{M_x}	8.3806×10^4 Ns
h_{F_x}	7.2019×10^3 Ns/m
h_{M_z}	-1.8948×10^5 Ns
h_{F_z}	4.0683×10^3 Ns/m
k_{M_x}	-3.7711×10^4 Nm
k_{F_x}	-6.1478×10^3 N
k_{M_z}	1.6174×10^5 Nm
k_{F_z}	-1.8306×10^3 N

The Coleman transformation and inverse are defined as follows [7].

$$
P = \begin{bmatrix}
1 & \sin(\varphi^{(1)}) & \cos(\varphi^{(1)}) \\
1 & \sin(\varphi^{(2)}) & \cos(\varphi^{(2)}) \\
1 & \sin(\varphi^{(3)}) & \cos(\varphi^{(3)})
\end{bmatrix},
$$

$$
P^{-1} = \begin{bmatrix}
\frac{1}{3} & \frac{1}{3} & \frac{1}{3} \\
\frac{2}{3}\sin(\varphi^{(1)}) & \frac{2}{3}\sin(\varphi^{(2)}) & \frac{2}{3}\sin(\varphi^{(3)}) \\
\frac{2}{3}\cos(\varphi^{(1)}) & \frac{2}{3}\cos(\varphi^{(2)}) & \frac{2}{3}\cos(\varphi^{(3)})
\end{bmatrix}.
$$

$$
\begin{aligned}
\begin{bmatrix} \delta\theta_{cm1}, & \delta\theta_{cm2}, & \delta\theta_{cm3} \end{bmatrix}^T &= P^{-1} \cdot \begin{bmatrix} \delta\theta_1, & \delta\theta_2, & \delta\theta_3 \end{bmatrix}^T, \\
\begin{bmatrix} \delta v_{cm1}, & \delta v_{cm2}, & \delta v_{cm3} \end{bmatrix}^T &= P^{-1} \cdot \begin{bmatrix} v_1, & v_2, & v_3 \end{bmatrix}^T, \\
\begin{bmatrix} \delta M_{cm1}, & \delta M_{cm2}, & \delta M_{cm3} \end{bmatrix}^T &= P^{-1} \cdot \begin{bmatrix} \delta M_1, & \delta M_2, & \delta M_3 \end{bmatrix}^T.
\end{aligned} \tag{6}
$$

For simulation purposes, the equations of motion are converted to discrete time using a zero-order hold discretization method with a sampling time of $0.01\ \mathrm{s}$. Denote the discrete time model by

$$
\begin{aligned}
x(k+1) &= A_{cm,d}x(k) + B_{cm,d}u_{cm}(k) + F_{cm,d}v_{cm}(k), \\
y_{cm}(k) &= C_{cm,d}x(k) + D_{cm,d}u_{cm}(k) + W_{cm,d}v_{cm}(k).
\end{aligned}
$$

Here, k discrete sampling instant. The subscript "d" represents discrete time. The transformation of the state space matrices to the discrete time can be found in standard modern control engineering textbooks, e.g. [9].

2.2 State observer for the wind turbine with additive faults

In this paper, we consider additive sensor or actuator faults in the wind turbine; i.e.

$$
\begin{aligned}
x(k+1) &= A_{cm,d}x(k) + B_{cm,d}u_{cm}(k) \\
&+ E_{cm,d}f_{cm}(k) + F_{cm,d}v_{cm}(k), \qquad (7) \\
y_{cm}(k) &= C_{cm,d}x(k) + D_{cm,d}u_{cm}(k) \\
&+ G_{cm,d}f_{cm}(k) + W_{cm,d}v_{cm}(k). \qquad (8)
\end{aligned}
$$

Here, $E_{cm,d} = B_{cm,d}, G_{cm,d} = D_{cm,d}$ for actuator faults; while $E_{cm,d} = 0, G_{cm,d} = I$, with appropriate dimensions for sensor faults.

Assume that v are zero mean white noise; hence so is v_{cm}. A Kalman filter for the LTI wind turbine model in the Coleman domain takes the following form,

$$\begin{aligned}\hat{x}(k+1) &= A_{cm,d}\hat{x}(k) + B_{cm,d}u_{cm}(k) \\ &+ E_{cm,d}f_{cm}(k) + K_{cm,d}e(k), \quad (9)\\ y_{cm}(k) &= C_{cm,d}\hat{x}(k) + D_{cm,d}u_{cm}(k) \\ &+ G_{cm,d}f_{cm}(k) + e(k). \quad (10)\end{aligned}$$

Here $e(k)$ is a zero mean white noise, or the so-called innovation signal, whose covariance, denoted by Σ_e, is determined by that of v_{cm} [10].

The closed-loop form of Eqs. (9,10) can then be rewritten as

$$\begin{aligned}\hat{x}(k+1) &= \Phi_{cm,d}\hat{x}(k) + \tilde{B}_{cm,d}u_{cm}(k) \\ &+ \tilde{E}_{cm,d}f_{cm}(k) + Ky_{cm}(k), \quad (11)\\ y_{cm}(k) &= C_{cm,d}\hat{x}(k) + D_{cm,d}u_{cm}(k) \\ &+ G_{cm,d}f_{cm}(k) + e(k), \quad (12)\end{aligned}$$

where $\Phi_{cm,d} = A_{cm,d} - K_{cm,d}C_{cm,d}, \tilde{B}_{cm,d} = B_{cm,d} - K_{cm,d}D_{cm,d}, \tilde{E}_{cm,d} = E_{cm,d} - K_{cm,d}G_{cm,d}$. This observer can be assumed to be asymptotically stable [10]. Since the fault signals f_{cm} are unknown, one cannot simulate the closed-loop observer (11,12). The faults will be dealt with in the next section.

3 Data driven FDI methodology

Modeling the wind turbine is an expensive and time consuming task. The effectiveness of the subspace model identification in identifying the wind turbine has been verified in [3, 11], with the wind speed disturbances v assumed as white noise. In this paper, we will show that the wind turbine model needs not to be identified for FDI purpose. Instead, FDI filters can be directly identified from I/O signals of the wind turbine.

Given a sequence of I/O signals, consecutively measured at N sampling instants, an output predictor in the following form of the fault-free plant with $f_{cm}(k) \equiv 0$ can be identified, provided that the input signals persistently excite ([4]) the wind turbine.

$$y_{cm}(k) = C_{cm,d}\Phi^s_{cm,d}\hat{x}(k-s) + \Xi_0 z^{k-1}_{k-s} + e(k). \quad (13)$$

Here, s is a positive integer, called the "past" horizon. With s large enough, $\Phi^s_{cm,d} = 0$, due to its stability. The initial condition term, $C_{cm,d}\Phi^s_{cm,d}\hat{x}(k-s)$, can hence be neglected.

$$\Xi_0 \triangleq \left[C_{cm,d}\Phi^{s-1}_{cm,d}\tilde{B}_{cm,d},\ C_{cm,d}\Phi^{s-1}_{cm,d}K_{cm,d},\ \cdots,\ C_{cm,d}\tilde{B}_{cm,d},\ C_{cm,d}K_{cm,d}\right]$$

contains a sequence of Markov parameters of the closed-loop observer form (11,12). The vector z^{k-1}_{k-s} collects a sequence of s past I/O samples; i.e. $z^{k-1}_{k-s} = \left[u^T_{cm}(k-s)\ y^T_{cm}(k-s)\ \cdots\ u^T_{cm}(k-1)\ y^T_{cm}(k-1)\right]^T$. Solving (13) in a least-squares (LS) sense results in an unbiased estimate $\hat{\Xi}_0$ and an estimated $\hat{\Sigma}_e$ [12].

With the identified Markov parameters in Ξ_0, an L-step output predictor with the additive faults, denoted by $\mathbf{y}_{k,L} = \left[y^T_{cm}(k-L+1)\ \cdots\ y^T_{cm}(k)\right]^T$, can be written as ([6])

$$\begin{aligned}\mathbf{y}_{k,L} &= \mathcal{H}_{s,u}\mathbf{u}_{k-L,s} + \mathcal{H}_{s,y}\mathbf{y}_{k-L,s} + \mathcal{T}_{L,u}\mathbf{u}_{k,L} \\ &+ \mathcal{T}_{L,y}\mathbf{y}_{k,L} + \mathcal{H}_{s,f}\mathbf{f}_{k-L,s} + \mathcal{T}_{L,f}\mathbf{f}_{k,L} + \mathbf{e}_{k,L}. \quad (14)\end{aligned}$$

Here $\mathbf{y}_{k-L,s} = \left[y^T_{cm}(k-s-L+1)\ \cdots\ y^T_{cm}(k-L)\right]^T$; and

$$\mathcal{H}_{s,\star} = \begin{bmatrix} C_{cm,d}\Phi^{s-1}_{cm,d}B_\star & C_{cm,d}\Phi^{s-2}_{cm,d}B_\star & \cdots & C_{cm,d}B_\star \\ C_{cm,d}\Phi^{s}_{cm,d}B_\star & C_{cm,d}\Phi^{s-1}_{cm,d}B_\star & \cdots & C_{cm,d}\Phi_{cm,d}B_\star \\ \vdots & \vdots & & \vdots \\ C_{cm,d}\Phi^{s+L-2}_{cm,d}B_\star & C_{cm,d}\Phi^{s+L-2}_{cm,d}B_\star & \cdots & C_{cm,d}\Phi^{L-1}_{cm,d}B_\star \end{bmatrix},$$

$$\mathcal{T}_{L,\star} = \begin{bmatrix} D_\star & & & \\ C_{cm,d}\tilde{B}_\star & D_\star & & \\ \vdots & \ddots & \ddots & \\ C_{cm,d}\Phi^{L-2}_{cm,d}\tilde{B}_\star & \cdots & C_{cm,d}\tilde{B}_\star & D_\star \end{bmatrix},$$

where with "$\star$" standing for "f, u, y", $B_\star$ and $D_\star$ respectively stands for $\tilde{E}_{cm,d}, \tilde{B}_{cm,d}, K_{cm,d}$ and $G_{cm,d}, D_{cm,d}, 0$.

Define the residual vector as

$$\begin{aligned}\mathbf{r}_k &= (I - \mathcal{T}_{L,y})\cdot\mathbf{y}_{k,L} - \mathcal{T}_{L,u}\cdot\mathbf{u}_{k,L} - \mathcal{H}_{s,u}\cdot\mathbf{u}_{k-L,s} \\ &- \mathcal{H}_{s,y}\cdot\mathbf{y}_{k-L,s} \quad (15)\\ &= \begin{bmatrix}\mathcal{H}_{s,f} & \mathcal{T}_{L,f}\end{bmatrix}\cdot\mathbf{f}_{k,s+L} + \mathbf{e}_{k,L}. \quad (16)\end{aligned}$$

The distribution of $\mathbf{r}_k$ belongs to the following parametric family [13].

$$\mathbf{r}_k \sim \begin{cases} \mathcal{N}(0, \mathcal{C}_e), & \text{fault free,} \\ \mathcal{N}(\begin{bmatrix}\mathcal{H}_{s,f} & \mathcal{T}_{L,f}\end{bmatrix}\cdot\mathbf{f}_{k,s+L}, \mathcal{C}_e), & \text{faulty.}\end{cases} \quad (17)$$

where $\mathcal{N}$ stands for normal distribution. $\mathcal{C}_e = I_L \otimes \Sigma_e$ is the covariance matrix of $\mathbf{r}_k$, where "$\otimes$" denotes Kronecker product. Standard χ^2 test can be applied to detect the change in the mean of $\mathbf{r}_k$ [6].

On the other hand, Eq. (15) defines an ill-posed least-squares problem for solving $\mathbf{f}_{k,s+L}$. It is proved in [6] that as $L \to \infty$, the following estimate of $f(k)$ is unbiased.

$$\hat{f}(k) = \underbrace{\mathcal{T}^{-1}_{L,f}\cdot\begin{bmatrix}-\mathcal{H}_{s,z} & \mathcal{T}_{L,u,y}\end{bmatrix}}_{\mathcal{F}}\cdot z_{k,s+L}, \quad (18)$$

where $\mathcal{H}_{s,z}$ denotes the Hankel matrix $\mathcal{H}_{s,\star}$ with $B_\star$ replaced by $\mathcal{B} = \begin{bmatrix}\tilde{B}_{cm,d}\ K_{cm,d}\end{bmatrix}$; while $z_{k,s+L}, \mathcal{T}_{L,u,y}$ are respectively defined as

$$\begin{bmatrix} u(k-L-s+1) \\ y(k-L-s+1) \\ \vdots \\ u(k) \\ y(k) \end{bmatrix}, \begin{bmatrix} \mathcal{D} & & & \\ -C\mathcal{B} & \mathcal{D} & & \\ \vdots & \vdots & \ddots & \\ -C\Phi^{L-2}_{cm,d}\mathcal{B} & -C\Phi^{L-3}_{cm,d}\mathcal{B} & \cdots & \mathcal{D} \end{bmatrix},$$

where $\mathcal{D} = [-D_{cm,d}\ I_\ell]$. $\mathcal{T}^{-1}_{L,f}$ is the inverse of $\mathcal{T}_{L,f}$, which is square and invertible in the case of sensor faults, provided that $A_{cm,d} - E_{cm,d}C_{cm,d}$ is stable [6].

In the case of actuator faults, $G_{cm,d} = 0$. We then need that $C_{cm,d}E_{cm,d}$ is square, and

$$A_{cm,d} - A_{cm,d}E_{cm,d}(C_{cm,d}E_{cm,d})^{-1}C_{cm,d}$$

is stable to guarantee (18) is asymptotically unbiased [6]. Unfortunately, $C_{cm,d}E_{cm,d}$ is not square in the wind turbine model. However, we can replace (12) with

$$\tilde{y}_{cm}(k) \triangleq U_{CE}^T y_{cm}(k) = U_{CE}^T \cdot \big[C_{cm,d}\hat{x}(k) + D_{cm,d}u_{cm}(k) + G_{cm,d}f_{cm}(k) + e(k)\big],$$

where U_{CE} is the range space of $C_{cm,d}E_{cm,d}$ from its SVD,

$$\begin{bmatrix} U_{CE} & U_{CE}^{\perp} \end{bmatrix} \begin{bmatrix} \Sigma_{CE} \\ 0 \end{bmatrix} V_{CE}^T. \tag{19}$$

The matrices $C_{cm,d}, D_{cm,d}, G_{cm,d}, \Sigma_e$ shall be respectively replaced by $U_{CE}^T C_{cm,d}, U_{CE}^T D_{cm,d}, U_{CE}^T G_{cm,d}$, $U_{CE}^T \Sigma_e U_{CE}$.

The matrix $\mathcal{F}$ defined in (18) contains a sequence of Markov parameters, from which the following fault estimation filter can be realized

$$x_{fe}(k+1) = A_{fe}x_{fe}(k) + B_{fe}z(k), \tag{20}$$
$$y_{fe}(k) = C_{fe}x_{fe}(k) + D_{fe}z(k), \tag{21}$$

where $z(k) = \begin{bmatrix} u(k) \\ y(k) \end{bmatrix}$. It is proved in [6] that the filter (20,21) are asymptotically equivalent to unknown input observers (UIOs).

4 Data driven FDI of the wind turbine model

In this section, we use the model introduced in Sec. 2 to simulate the wind turbine. The I/Os collected from the simulation are used for the data driven FDI designs introduced in Sec. 3.

The open-loop wind turbine is not asymptotically stable, which contains an integrator. A collective pitch controller in a feedback loop is added to stabilize the system. The controller used can be found in [8]. Extra excitation signals $r_{\delta\theta_1}, r_{\delta\theta_2}, r_{\delta\theta_3}, r_{\delta T_{ge}}$ were superimposed onto the pitch-angle inputs, defined as follows.

- $r_{\delta\theta_2}, r_{\delta\theta_3} \equiv 0$,[1]
- $r_{\delta\theta_1}$ as a zero-mean white noise with a variance of 100, low-passed with a cut-off frequency of $4.5176 rad/s$.
- $r_{\delta T_{ge}}$ as a zero-mean white noise with a variance of 10^6, low-passed with a cut-off frequency of $0.2\pi(rad/s)$.

The wind speed disturbances along x, y, z directions are respectively chosen as low pass filtered zero-mean white noise with a variance of 2, whose spectrums are shown in Fig. 2. This does not conflict with the white noise assumption of v in the data-driven algorithms, because the filter dynamics can be embedded into the identified innovation type output predictor.

[1] Since in reality, they cannot be excited.

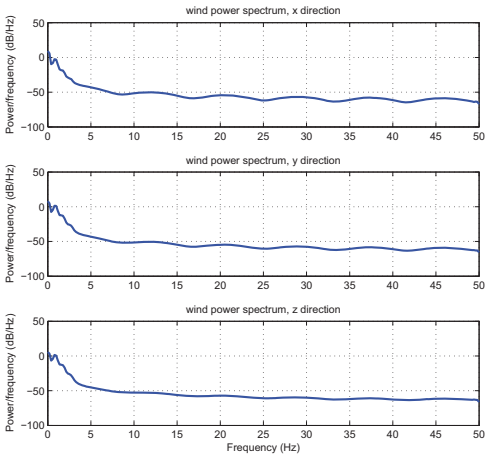

Figure 2: The spectrum of the wind speed disturbances.

The I/Os are transformed into the Coleman domain by (6). The parameters in the data driven FDI designs are chosen as follows:

- the detection horizon $L = 3$ for fault detection,
- the detection horizon $L = 100$ for fault estimation,
- the past horizon $s = 20$,
- the false alarm rate $\alpha = 10^{-5}$ for the hypothesis test of fault detection,
- 3000 I/O samples for identification.

The identification signals are scaled such that the covariance of both the inputs and the outputs is unity. Note that due to the poorly excited wind turbine, the least-squares problem (13) is regularized by a factor of $\rho = 100$.

Consider the drifting fault of the sensor measuring the collective blade root moment M_{z1}; i.e.

$$f_{M_{z1}}(k) = \begin{cases} 0, & k < t_1, \\ 10^6 \cdot \frac{k-t_1}{t_2-t_1} & t_1 \le k < t_2. \end{cases}$$

Figure 3 illustrates the fault detection result of the identified residual generator defined by (15). The successful classification rate is 100%.

Figure 4 illustrates the fault estimation result of the data-driven FICSI, by the identified estimation filter (20,21). The stability of $A_{cm,d} - E_{cm,d}C_{cm,d}$ is automatically satisfied by the wind turbine model. The tornado-shaped curve is due to the inverse Coleman transformation (6). Clearly, the fault estimates are unbiased.

As one more case study to detect actuator faults, consider a constant bias fault on the variation in the generator torque δT_{ge}; i.e.

$$f_{\delta T_{ge}}(k) = \begin{cases} 0, & k < t_1, \\ 3 \times 10^6 \cdot \frac{k-t_1}{t_2-t_1} & t_1 \le k < t_2. \end{cases}$$

Figure 5 illustrates the fault detection result of the identified residual generator defined by (15). The successful classification rate is 99.8%.

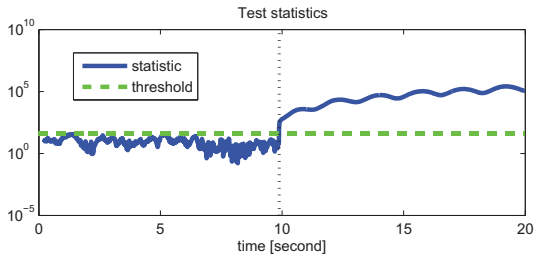

Figure 3: Fault detection by the identified FICSI fault detection filter, with $s = 20, L = 3$.

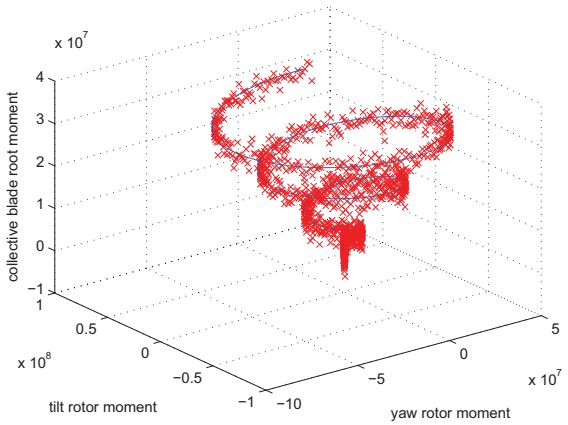

Figure 4: Fault estimation by the identified FICSI fault estimation filter, with $s = 20, L = 100$.

5 Conclusions

In this paper, we have studied a data driven FDI filter design approach for LTI systems on a large-scale wind turbine. This approach does not require modeling its dynamics; but instead, identifies detection and asymptotically unbiased estimation filters directly from the I/O signals of the turbine. The wind turbine under consideration is described by a seventh order nonlinear state space model. To deal with its nonlinearity, the I/O signals of the turbine are transformed into the Coleman domain, where its dynamics correspond to an LTI model. Due to the current limitation in the identification of the output predictor, it shall be an attractive extension of the developed FDI algorithms to handle other types of disturbances in the future work, e.g. periodic disturbances.

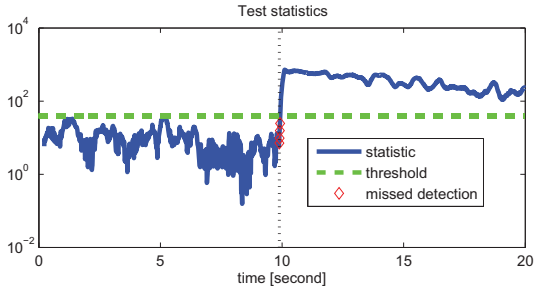

Figure 5: Fault detection by the identified FICSI fault detection filter, with $s = 20, L = 3$.

References

[1] P. Caselitz, J. Giebhardt, T. Krüger, and M. Mevenkamp. Development of a fault detection system for wind energy converters. In *the Proceedings of the EUWEC*. Göteborg, 1996.

[2] P. Caselitz, J. Giebhardt, M. Mevenkamp, and M. Reichardt. Application of condition monitoring systems in wind energy converters. In *the Proceedings of the EWEC*. Dublin, 1997.

[3] X. Wei, M. Verhaegen, and T. van den Engelen. Sensor fault detection and isolation for wind turbines based on subspace identifcation and kalman filter techniques. *International Journal of Adaptive Control and Signal Processing. To appear*, 2009.

[4] M. Verhaegen and V. Verdult. *Filtering and System Identification: A Least Squares Approach*. Cambridge University Press, 2007.

[5] J. Dong and M. Verhaegen. Subspace based fault identification for LTI systems. In *the Proceedings of the 7th IFAC Symposium on Fault Detection, Supervision and Safety of Technical Processes (SafeProcess09)*, pages 330–335. Barcelona, Spain, 2009.

[6] J. Dong. *Data driven fault tolerant control: a subspace approach*. PhD thesis, Delft University of Technology, 2009.

[7] T.G. Engelen. Design model and load reduction assessment for multi-rotational mode individual pitch control. In *the Proceedings of European Wind Energy Conference (EWEC2006)*. Athens, Greece, 2006.

[8] T. van Engelen, H. Markou, T. Buhl, and B. Marrant. Morphological study of aeroelastic control concepts for wind turbines. Technical report, Energy Research Center (ECN), 2007.

[9] K.J. Åström and B. Wittenmark. *Computer controlled systems: theory and design*. Prentice Hall, 1984.

[10] L. Ljung. *System Identification - Theory for the User*. Prentice-Hall, Englewood Cliffs, 1987.

[11] J.W. van Wingerden, I. Houtzager, F. Felici, and M. Verhaegen. Closed-loop identification of the time-varying dynamics of variable speed wind turbines. *International Journal of Robust and Nonlinear Control*, 19:4–21, 2009.

[12] A. Chiuso. On the relation between CCA and predictor-based subspace identification. *IEEE Transactions on Automatic Control*, 52:1795–1812, 2007.

[13] M. Basseville. On fault detectability and isolability. *European Journal of Control*, 7:625–638, 2001.